Physica A 450 (2016) 1–17

Contents lists available at ScienceDirect

Physica A

journal homepage: www.elsevier.com/locate/physa

Signals on graphs: Transforms and tomograms

R. Vilela Mendes [a,*], Hugo C. Mendes [b], Tanya Araújo [c]

[a] Centro de Matemática e Aplicações and Instituto de Plasmas e Fusão Nuclear, University of Lisbon, Faculdade de Ciências, C6 - Piso 1, 1749-016 Lisboa, Portugal

[b] Instituto Português do Mar e da Atmosfera, Avenida Brasília, 1300-598 Lisboa, Portugal

[c] Instituto Superior de Economia e Gestão, University of Lisbon, Rua do Quelhas, 6, 1200-781, Lisboa, Portugal

HIGHLIGHTS

- A general framework for graph signal transforms.
- A correct generalization of the notion of wavelet transform to graphs.
- The construction of the graph tomogram transforms.

ARTICLE INFO

Article history:
Received 29 October 2015
Available online 13 January 2016

Keywords:
Network signals
Graph-transforms
Tomograms
Dynamics on networks

ABSTRACT

Development of efficient tools for the representation of large datasets is a precondition for the study of dynamics on networks. Generalizations of the Fourier transform on graphs have been constructed through projections on the eigenvectors of graph matrices. By exploring mappings of the spectrum of these matrices we show how to construct more general transforms, in particular wavelet-like transforms on graphs. For time-series, tomograms, a generalization of the Radon transforms to arbitrary pairs of non-commuting operators, are positive bilinear transforms with a rigorous probabilistic interpretation which provide a full characterization of the signals and are robust in the presence of noise. Here the notion of tomogram is also extended to signals on arbitrary graphs.

1. Introduction

The analysis of evolving data on complex networks is an emerging topic of current interest in physics and many other fields. Work in this field appears in several flavors. Some authors concern themselves with relations and connectedness, that is, with the community structure, others with the role of particular network vertices. A topic of relevance is the impact of network structure on the diffusion of information, imitation, failure propagation and all kinds of dynamical behaviors of the system. Reference models like random graphs, Poisson graphs, scale free graphs, etc. are regularly used to quantify the network characteristics, by using parameters which include clustering coefficients, path length, diameter and centralities. Inference and learning from large network-based datasets is also a topic of current interest.

Prior to the description of dynamical systems defined on graphs, or the dynamics of the graph itself, is the construction of efficient representations for these large datasets. Earlier works used spectral graph theory and the graph Laplacian [1] to derive low-dimensional representations by projecting the data on low-dimensional subspaces associated to subsets of the Laplacian eigenvectors. More recently some authors have proposed transforms for data indexed by graphs. In particular,

* Corresponding author.
E-mail addresses: rvmendes@fc.ul.pt, rvilela.mendes@gmail.com (R. Vilela Mendes), hugart@gmail.com (H.C. Mendes), tanya@iseg.utl.pt (T. Araújo).

http://dx.doi.org/10.1016/j.physa.2016.01.002
0378-4371/

generalizations of the Fourier transform have been proposed [2–4] which are used to extend to graphs many of the signal processing concepts used for time series [5–7]. Typically, these transforms make a change of basis from the vertex space to some other space of vectors which is then used to project the graph signal. They are the analog of linear transforms in time series. So far as we know, the question of multiple feature characterization of graph signals, for example bilinear transforms, has not been addressed in the past. For time series it is known that bilinear transforms, like Wigner–Ville, have serious interpretation problems. However the recently developed tomographic framework [8–11] allows for a probabilistically robust multiple feature characterization of time signals. The correct generalization of the notion of wavelet transforms to graphs and the extension of the tomographic framework to graph signals are the main contributions of this paper.

In Section 2, to set notation, we review the notions of linear, bilinear and tomographic transforms for time signals. In Section 3, transforms and tomograms for static and dynamical data on graphs are introduced and in Section 4 some illustrative examples are worked out.

2. Signal transforms for time series: Linear, quasi-distributions and tomograms

The traditional field of signal processing deals mostly with the analysis of time series. Signal processing of time series relies heavily on integral transforms [12,13]. Three types of transforms have been used: linear, bilinear and tomograms. Among the linear transforms, Fourier and wavelets are the most popular. The Fourier transform extracts the frequency components of the signal and the wavelets its multiscale nature. However, this is achieved at the expense of the time information, in the sense that the time location of the frequency components and of the scale features is lost in the process. This motivated the development of bilinear transforms like the time–frequency Wigner–Ville [14,15] or the frequency–scale Bertrand [16,17] quasidistributions. The aim of the Wigner–Ville transform was to provide joint information on the time–frequency plane, an important issue because, in many applications (biomedical, seismic, radar, etc.), the nature of the signals may change on short time scales. However, the oscillating cross-terms in the Wigner–Ville and other quasidistributions [18–20] render the interpretation of the transformed signals a difficult matter. Even when the average of the cross-terms is small, their amplitude may be large in time–frequency regions that carry no physical information.

The difficulties with the physical interpretation of quasidistributions arise from the fact that time and frequency (or frequency and scale) are noncommutative operator pairs. Hence, a joint probability density can never be defined. Even in the case of positive quasiprobabilities like the Husimi–Kano function [21,22], an interpretation as a joint probability distribution is also not possible because the two arguments in the function are not simultaneously measurable random variables. More recently, a new type of strictly positive bilinear transform has been proposed [8–10], called a tomogram, which is a generalization of the Radon transform [23] to arbitrary noncommutative pairs of operators. The Radon–Wigner transform [24,25] is a particular case of the noncommutative tomography technique. Being strictly positive densities, the tomograms provide a full characterization of the signal and are robust in the presence of noise.

A unified framework to characterize linear transforms, quasidistributions and tomograms was developed in Ref. [9]. In finite dimensional spaces a signal f may be represented as a column vector and the scalar product as $g^T f$, the transposed g^T being a row vector. However in infinite-dimensional spaces $\mathcal{N}$ and when f is not normalizable the notion of scalar product loses its meaning and is better to use the notation $|f\rangle$ and $\langle g|$ to emphasize that g belongs to a smaller space (the dual $\mathcal{N}^*$ of $\mathcal{N}$). Then, the notation $\langle g \mid f\rangle$, the value of the functional $\langle g|$ on the vector $|f\rangle$, generalizes the notion of scalar product when the space of the $\langle g|$'s and the $|f\rangle$'s cannot be identified. Also $\langle g|\, U\, |f\rangle$ means the action of the operator U on $|f\rangle$ and then the evaluation of the functional $\langle g|$ on the new vector [26].

Consider now a signal $f(t)$ as a vector $|f\rangle$ in a subspace $\mathcal{N}$ of a Hilbert space $\mathcal{H}$, a family of unitary operators $U(\alpha) = \mathrm{e}^{\mathrm{i}B(\alpha)}$ and a reference vector h in the dual $\mathcal{N}^*$ of $\mathcal{N}$. A linear transform like Fourier or wavelet is

$$W_f^{(h)}(\alpha) = \langle U(\alpha)\, h \mid f\rangle \tag{1}$$

and a quasidistribution is

$$Q_f(\alpha) = \langle U(\alpha) f \mid f\rangle. \tag{2}$$

To define the tomogram let, in the unitary operator $U(\alpha) = \mathrm{e}^{\mathrm{i}B(\alpha)}$, $B(\alpha)$ have the spectral decomposition $B(\alpha) = \int XP(X)\,\mathrm{d}X$, where $P(X)$ denotes the projector on the (generalized) eigenvector $\langle X| \in \mathcal{N}^*$ of $B(\alpha)$. The tomogram is

$$M_f^{(B)}(X) = \langle f|\, P(X)\, |f\rangle = |\langle X \mid f\rangle|^2. \tag{3}$$

The tomogram $M_f^{(B)}(X)$ is the squared amplitude of the projection of the signal $|f\rangle \in \mathcal{N}$ on the eigenvector $\langle X| \in \mathcal{N}^*$ of the operator $B(\alpha)$. Therefore it is positive. For normalized $|f\rangle$,

$$\langle f \mid f\rangle = 1$$

the tomogram is normalized

$$\int M_f^{(B)}(X)\ \mathrm{d}X = 1 \tag{4}$$

and may be interpreted as a probability distribution on the set of generalized eigenvalues of $B(\alpha)$, that is as the probability distribution for the variable X corresponding to the observable defined by the operator $B(\alpha)$.

For example, if the unitary $U(\alpha)$ is generated by $B_F(\alpha) = \alpha_1 t + \mathrm{i}\alpha_2 \frac{\mathrm{d}}{\mathrm{d}t}$ and h is a (generalized) eigenvector of the time-translation operator, the linear transform $W_f^{(h)}(\alpha)$ is the Fourier transform. For the same $B_F(\alpha)$, the quasi-distribution $Q_f(\alpha)$ is the ambiguity function and the Wigner–Ville transform [14,15] is the quasi-distribution $Q_f(\alpha)$ for the following B-operator

$$B^{(WV)}(\alpha_1, \alpha_2) = -\mathrm{i}2\alpha_1 \frac{\mathrm{d}}{\mathrm{d}t} - 2\alpha_2 t + \frac{\pi\left(t^2 - \frac{\mathrm{d}^2}{\mathrm{d}t^2} - 1\right)}{2}. \tag{5}$$

The wavelet transform is the linear transform $W_f^{(h)}(\alpha)$ for $B_W(\alpha) = \alpha_1 D + \mathrm{i}\alpha_2 \frac{\mathrm{d}}{\mathrm{d}t}$, D being the dilation operator $D = -\frac{1}{2}\left(\mathrm{i}t\frac{\mathrm{d}}{\mathrm{d}t} + \mathrm{i}\frac{\mathrm{d}}{\mathrm{d}t}t\right)$. The wavelets $h_{s,\tau}(t)$ are kernel functions generated from a basic wavelet $h(\tau)$ by means of a translation and a rescaling ($-\infty < \tau < \infty,\ s > 0$):

$$h_{s,\tau}(t) = \frac{1}{\sqrt{s}} h\left(\frac{t-\tau}{s}\right) \tag{6}$$

using the operator

$$U^{(A)}(\tau, s) = \exp\left(-\tau\frac{\mathrm{d}}{\mathrm{d}t}\right)\exp(\mathrm{i}\log sD), \tag{7}$$

$$h_{s,\tau}(t) = U^{(A)\dagger}(\tau, s)h(t). \tag{8}$$

The Bertrand transform [16,17] is the quasi-distribution $Q_f(\alpha)$ for B_W. Linear, bilinear and tomogram transforms are related to one another [9].

As stated before, tomograms are obtained from projections on the eigenstates of the B operators. These operators may be linear combinations of different (commuting or noncommuting) operators O_1 and O_2,

$$B = \mu O_1 + \nu O_2 \tag{9}$$

meaning that the tomogram explores the signal along lines in the plane (O_1, O_2). For example for

$$B(\mu, \nu) = \mu t + \nu\omega = \mu t + \mathrm{i}\nu\frac{\mathrm{d}}{\mathrm{d}t} \tag{10}$$

($\omega = \mathrm{i}\frac{\mathrm{d}}{\mathrm{d}t}$) the tomogram is the expectation value of a projection operator with support on the line in the time–frequency plane

$$X = \mu t + \nu\omega. \tag{11}$$

Therefore, $M_f^{(S)}(X, \mu, \nu)$ is the marginal distribution of the variable X along this line in the time–frequency plane. The line is rotated and rescaled when one changes the parameters μ and ν. In this way, the whole time–frequency plane is sampled and the tomographic transform contains all the information on the signal. *The probabilistic nature of the tomogram implies that, in contrast with quasi-distributions, the information thus obtained is robust and unambiguous.*

Tomograms associated to linear combinations of time with the generators of the conformal group ($\mathrm{i}\frac{\mathrm{d}}{\mathrm{d}t}$; $\mathrm{i}\left(t\frac{\mathrm{d}}{\mathrm{d}t} + \frac{1}{2}\right)$; $\mathrm{i}\left(t^2\frac{\mathrm{d}}{\mathrm{d}t} + t\right)$) and several other known operators have been explored [10]. By providing a robust extraction of compound signal features, tomograms have been useful in denoising, component separation and structure identification [11,27–31].

Notice that the notion of tomogram provides a probabilistic robust characterization of any number of signal characteristics. For example, instead of a linear combination of two operators as in (9), we may project on the eigenvectors of a linear (or nonlinear) combination of any number of operators. For a detailed theory of the tomogram transforms and, in particular, their mathematical status as operator symbols we refer to Refs. [9,10].

3. Signal transforms and tomograms on graphs

From the graph point of view a time series is a signal on a one-dimensional directed graph with vertices labeled by the times $(t_0, t_1, t_2, \ldots)$ and the edges connecting t_{k+1} to t_k. That is, the adjacency matrix $\mathbf{A}$ of a time series is, in general

$$\mathbf{A} = \begin{pmatrix} 0 & 0 & 0 & 0 & \cdots \\ 1 & 0 & 0 & 0 & \cdots \\ 0 & 1 & 0 & 0 & \cdots \\ 0 & 0 & 1 & 0 & \cdots \\ \vdots & \vdots & \vdots & \vdots & \cdots \end{pmatrix} \tag{12}$$

or, for a time-periodic signal

$$\mathbf{A} = \begin{pmatrix} 0 & 0 & 0 & \cdots & 0 & 1 \\ 1 & 0 & 0 & \cdots & 0 & 0 \\ 0 & 1 & 0 & \cdots & 0 & 0 \\ 0 & 0 & 1 & \cdots & 0 & 0 \\ \vdots & \vdots & \vdots & \vdots & 0 & 0 \\ 0 & 0 & 0 & 0 & 1 & 0 \end{pmatrix}. \tag{13}$$

As discussed before, linear signal transforms for a time series are projections on the set of eigenvectors of a linear operator. These operators are not arbitrary, but chosen to extract particular features of the signal that is being analyzed. The Fourier transform looks for periodic features, wavelets for multiscale features, etc. Likewise, useful information from signals on arbitrary graphs may be obtained from projections on sets of vectors associated to suitably chosen linear operators. For the time-periodic signal, it is easy to see that the discrete Fourier transform is the projection on the eigenvectors of the adjacency matrix (13). Therefore one may generalize the notion of Fourier transform for graphs as the projection on the eigenvectors (or on the generalized eigenvectors of the Jordan decomposition) of the adjacency matrix. This was the point of view taken by some authors [4–6] to develop a theory of discrete signal processing on graphs. However this choice is not unique because, for the time series network other matrices have the same spectrum, for example the Laplacian matrix

$$\mathbf{L} = \mathbf{D} - \mathbf{A}$$

D being the degree matrix, which for the time series is the identity. Hence, the graph Fourier transform might as well be defined as a projection on the generalized eigenvectors of the Laplacian matrix [2,3,7,32]. This operator point of view allows not only to generalize the notion of transforms but also the notions of filtering and other general linear operations on graph signals.

Now a generalization of the notions of linear transform and tomogram, for signals on graphs, will be developed. Generalization of the notion of bilinear transform will not be dealt with because, already for time series, it leads to difficult interpretation problems.

3.1. Graph transforms

Let $G = (\mathcal{V}, \mathbf{A})$ be a graph, with $\mathcal{V} = \{v_0, \ldots, v_{N-1}\}$ the set of vertices and **A** the weighted adjacency matrix. Each matrix element $\mathbf{A}_{n,m}$ is the weight of a directed edge from v_m to v_n which can take arbitrary real or complex values. $\mathcal{N}_n = \{m \mid \mathbf{A}_{n,m} \neq 0\}$ is the neighborhood of v_n and a graph signal is a map $\mathbf{f} = \{f_n\}$ from the set $\mathcal{V}$ of vertices into the set of complex numbers $\mathbb{C}$, each element f_n being indexed by the vertex v_n.

Other useful graph matrices are:

- *The degree matrix* **D**: a diagonal matrix listing the degree of the vertices
- *The symmetrically normalized Laplacian matrix*: $\mathbf{L}' = \mathbf{D}^{-\frac{1}{2}}\mathbf{L}\mathbf{D}^{-\frac{1}{2}}$
- *The random walk matrix*: $\mathbf{W} = \mathbf{A}\mathbf{D}^{-1}$
- *The lazy random walk matrix*: $\mathbf{W}' = \left(\mathbf{I} + \mathbf{A}\mathbf{D}^{-1}\right)/2$
- *The incidence matrix* **E**: is the $N_e \times N$ matrix (N_e = no. edges, N = no. of vertices) given by

$$\mathbf{E}_{e,v} = \begin{cases} 1 & \text{if} \quad e = (v, w) \quad \text{and } v < w \\ -1 & \text{if} \quad e = (v, w) \quad \text{and } v > w \\ 0 & \quad \text{otherwise} \qquad\quad . \end{cases}$$

- *The edge adjacency matrix*: is a $N_e \times N_e$ matrix determined by the adjacencies of edges

$${}^{e}\mathbf{A}_{i,j} = \begin{cases} 1 & \text{if edges } i \text{ and } j \text{ are adjacent} \\ 0 & \text{otherwise.} \end{cases}$$

These matrices have been used in the past mostly to characterize the topological structure of networks, for vertex clustering, for the detection of communities, etc. [1,33–37]. Here they will be considered as operators which generate a set of (generalized) eigenvectors to project the signals on graphs.

3.1.1. Fourier-like transforms

Denote any one of the $N \times N$ graph matrices by **M**. The matrices **M** act on the space of graph signals by

$$f_n \to \widetilde{f}_n = \sum_m \mathbf{M}_{n,m} f_m = \sum_{m \in \mathcal{N}_n} \mathbf{M}_{n,m} f_m. \tag{14}$$

When the matrix **M** is the adjacency matrix this operation generalizes the notion of time shift, when time sequences are looked at as forward-connected graphs.

For many real-world datasets the matrices $\mathbf{M}$ are not diagonalizable. In those cases, to obtain a suitable set of expansion vectors one may either use the symmetric combinations $\mathbf{M}\mathbf{M}^T$ and $\mathbf{M}^T\mathbf{M}$ to generate an expansion basis or, alternatively, use the block-diagonal Jordan decomposition of $\mathbf{M}$.

$$\mathbf{M} = \mathbf{V}\mathbf{J}\mathbf{V}^{-1} \tag{15}$$

$$\mathbf{J} = \begin{pmatrix} J_{R_{0,0}}(\lambda_0) & & \\ & \ddots & \\ & & J_{R_{M-1,D_{M-1}}}(\lambda_{M-1}) \end{pmatrix} \tag{16}$$

with Jordan blocks associated to the eigenvalues of $\mathbf{M}$

$$\mathbf{J}_{r_{m,d}}(\lambda_m) = \begin{pmatrix} \lambda_m & 1 & & \\ & \lambda_m & \ddots & \\ & & \ddots & 1 \\ & & & \lambda_m \end{pmatrix}. \tag{17}$$

The columns of the matrix $\mathbf{V}$, that brings $\mathbf{M}$ to its Jordan normal form, are the eigenvectors

$$(\mathbf{M} - \lambda_m \mathbf{I})\mathbf{v}_{m,d,0} = 0 \tag{18}$$

and the generalized eigenvectors of the Jordan chain

$$(\mathbf{M} - \lambda_m \mathbf{I})\mathbf{v}_{m,d,r} = \mathbf{v}_{m,d,r-1} \tag{19}$$

of $\mathbf{M}$. These vectors may then be used to project the signals on the graph and, considering the graph signal $\mathbf{f}$ as a column vector, the $\mathbf{M}$-transform is

$$\widehat{\mathbf{f}} = \mathbf{V}^{-1}\mathbf{f} \tag{20}$$

with inverse transform

$$\mathbf{f} = \mathbf{V}\widehat{\mathbf{f}}. \tag{21}$$

As stated before, when $\mathbf{M}$ is either the adjacency or the Laplacian matrix, the transforms so obtained correspond to the graph generalization of the Fourier transform as proposed by several authors [2–7,32]. When the matrices are not symmetric, the problem with these transforms lies in the fact that in general the set of generalized eigenvectors do not form an orthogonal basis. Therefore it is sometimes more convenient to use $\mathbf{M}\mathbf{M}^T$ and $\mathbf{M}^T\mathbf{M}$ to generate the expansion basis, leading to what we will call the $\mathbf{M}\mathbf{M}^T$- or $\mathbf{M}^T\mathbf{M}$-transform.

3.1.2. Wavelet-like transforms

The definition of wavelet-like transforms for graphs requires a more elaborate construction. For time series the affine wavelets use, in Eq. (1), an operator $U(\alpha)$ consisting of the product of a translation and a scale transformation which act on a fixed reference signal (the mother wavelet $h_0(t)$), namely

$$\begin{aligned} h_{s,a}(t) &= U(s,a)\, h_0(t) = \mathrm{e}^{\log s\left(t\frac{\mathrm{d}}{\mathrm{d}t}+\frac{1}{2}\right)}\mathrm{e}^{a\frac{\mathrm{d}}{\mathrm{d}t}} h_0(t) \\ &= \sqrt{s} h_0(st+a)\,. \end{aligned} \tag{22}$$

Translation in the graph is easily generalized but it is not obvious how to generalize scale transformations. This becomes clearer if we rewrite the wavelet transform in frequency space,

$$\begin{aligned} f(a,s) &= \int \mathrm{d}t h^*_{s,a}(t) f(t) \\ &= \int \mathrm{d}t \left(\mathrm{e}^{\log s\left(t\frac{\mathrm{d}}{\mathrm{d}t}+\frac{1}{2}\right)}\mathrm{e}^{a\frac{\mathrm{d}}{\mathrm{d}t}} h^*_0(t)\right) f(t) \\ &= \int \mathrm{d}\omega \frac{\mathrm{e}^{-\mathrm{i}\frac{\omega}{s}a}}{\sqrt{s}} \widehat{h}^*_0\left(\frac{\omega}{s}\right)\widehat{f}(\omega) \end{aligned} \tag{23}$$

$\widehat{h}_0$ and $\widehat{f}$ denoting the Fourier transforms of the mother wavelet and of the signal. One sees that the wavelet transform is represented as a sum over the Fourier spectrum Ω with the (frequency) argument of the mother wavelet shifted from ω to $\frac{\omega}{s}$. The mapping $\omega \in \Omega \to \frac{\omega}{s} \in \Omega$ is a one-to-one onto mapping of the Fourier spectrum Ω into itself. Therefore the natural generalization of the wavelet transform for graphs may be defined as a similar sum, with the spectrum label shift being one of the possible one-to-one onto mappings of the spectrum of the adjacency matrix (or of the Laplacian matrix).

Writing the Fourier-like transform on graphs and its inverse as

$$\widehat{f}(\eta) = \sum_i \chi_\eta(i) f(i)$$
$$f(i) = \sum_\eta \widehat{f}(\eta)\, \chi_\eta(i) \tag{24}$$

where $\chi_\eta(i)$ is an eigenvector of $\mathbf{A}$ or $\mathbf{L}$ (or a generalized eigenvector or an eigenvector of $\mathbf{A}^T\mathbf{A}$ or $\mathbf{L}^T\mathbf{L}$) and η denotes the spectral label in the spectrum Ω of the matrices. With a localized "mother wavelet"

$$h^{(k)}(i) = \delta_{k,i} \tag{25}$$

the wavelet-like transform on graphs would be

$$f(a, \widetilde{s}) = \sum_\eta \chi_{\widetilde{s}(\eta)}(k+a)\widehat{f}(\eta)\,. \tag{26}$$

The mapping $\widetilde{s}(\eta)$ is not $\eta \to \frac{\eta}{s}$ because in general $\frac{\eta}{s}$ is not in Ω. $\widetilde{s}$ is a mapping in the set $\mathcal{S}$ of the possible one-to-one onto mappings of Ω, $\widetilde{s} \in \mathcal{S}$.

The inverse wavelet transform is

$$\widehat{f}(\eta) = \frac{1}{\#\mathcal{S}} \sum_{a,\widetilde{s}} \chi_{\widetilde{s}(\eta)}(a) f\left(a, \widetilde{s}\right). \tag{27}$$

$\#\mathcal{S}$ denoting the cardinality of $\mathcal{S}$.

Hammond, Vandergheynst and Gribonval [38] have also attempted to generalize the notion of wavelet transform to graph signals. However, instead of the sum with the shifted arguments in the spectrum, their construction corresponds to the introduction of a η-dependent weight on the sum of the 2nd equation in (24), with both the signal component $\widehat{f}(\eta)$ and the eigenvector χ_η associated to the same spectral value η. Therefore their construction is more in the spirit of a Fourier deformation of the signal rather than of a wavelet transform.

An even more general transform would be

$$f(a, C) = \sum_{\eta,\eta'} C\left(\eta, \eta'\right) \chi_{\eta'}(a) \widehat{f}(\eta)\,. \tag{28}$$

For comparison with the time series case, this last construction would be similar to the case of "conformal wavelets" generated by $e^{\alpha\left(t^2\frac{d}{dt}+t\right)} e^{a\frac{d}{dt}} h_0(t)$.

In time series, times are labels on the data, therefore it is natural to frame time series as graphs, times being the vertices of the graph. The time-series-as-graph analogy was also the one used by previous authors in their generalization of the Fourier transform. However, the construction could as well start from the notions used to describe multidimensional spatial signals. But whatever starting point is used, the formulation of the general theory of graph signal processing might (and should) also have an impact on the classical treatment of spatial signals. For example, some algorithms in image processing convert the image to a linear signal, thus neglecting the global metric relations of the adjacency matrix. Also, transforms much more general than the 2D Fourier transform are easier to construct on a graph-based setting.

3.2. Graph tomograms

So far, signals on graphs have been described either as vectors on vertex space or as projections of these vectors on the generalized eigenvectors of a particular matrix $\mathbf{M}$. Each particular matrix emphasizes a specific topological property of the graph. As in time series, tomograms for graphs are designed to obtain information about more than one signal feature by projecting on the generalized eigenvectors of a matrix that interpolates between two distinct matrices $\mathbf{M}_1$ and $\mathbf{M}_2$. This parallels what for time series is achieved, for example, by the time–frequency tomogram.

In a time series the successive times $t_1, t_2 \ldots t_n$ are the eigenvalues of the time operator t that appears in $B_F(\alpha) = \alpha_1 t + i\alpha_2 \frac{d}{dt}$, the $B_F(\alpha)$ operator that generates the time–frequency tomogram. For a graph the corresponding notion is the *vertex operator*. For a graph with N vertices the *vertex operator* is

$$\mathbf{T} = \begin{pmatrix} 1 & 0 & 0 & \vdots & 0 \\ 0 & e^{i\frac{2\pi}{N}} & 0 & \vdots & 0 \\ 0 & 0 & e^{i\frac{2\pi}{N}\times 2} & \vdots & 0 \\ \cdots & \cdots & \cdots & \ddots & \vdots \\ 0 & 0 & 0 & \cdots & e^{i\frac{2\pi}{N}\times(N-1)} \end{pmatrix} \tag{29}$$

and the vertex signal $\mathbf{f} = \{f_n\}$ corresponds to a projection of the signal $\mathbf{f}$ on the eigenvectors of this operator. Therefore, the construction of a tomogram for graph signals would amount to finding an operator that interpolates between $\mathbf{T}$ and one of the matrices $\mathbf{M}$ listed before. A possible solution would be

$$B_\alpha = (1-\alpha)\,\mathbf{T} + \alpha\mathbf{M} \tag{30}$$

with α varying between 0 and 1, the tomogram being obtained by the projections of the signal $\mathbf{f}$ on the eigenvectors of B_α. If $\mathbf{M}$ is the adjacency matrix $\mathbf{A}$, this construction, interpolating between $\mathbf{A}$ and the vertex operator $\mathbf{T}$ is, for graphs, the analog of the time–frequency tomogram.

Even if the ordering of the vertices is arbitrary, the vertex operator is always a meaningful entity in the sense that if, for example, the tomogram is used for clustering purposes, it is the $\mathbf{T}$ operator that allows to identify which vertices belong to each cluster. In addition some additional information may be introduced into $\mathbf{T}$ by using for example geographical ordering of the nodes, or some other property.

Tomograms may also be constructed by using two of the listed $\mathbf{M}$ matrices

$$B_\alpha = (1-\alpha)\,\mathbf{M}_1 + \alpha\mathbf{M}_2$$

which may be used to refine the analysis beyond the information obtained from the $\mathbf{T}$, $\mathbf{M}$-tomogram.

As discussed before, the reason why time and frequency cannot be simultaneously specified is because they correspond to a pair of non-commuting operators. This is the reason why bilinear transforms, like Wigner–Ville, are unreliable and it is also the main motivation for using tomogram transforms. In graphs, the vertex description and the adjacency matrix projection are also incompatible specifications, because in general the $\mathbf{T}$ and $\mathbf{A}$ (or $\mathbf{L}$) matrices do not commute. It is in this sense, that, as recently stated [32,39], there is an uncertainty principle for graphs, that is, a fundamental trade-off between a signal localization on the graph and on its spectral domain.

3.3. Tomograms and dynamics

The graph tomogram, as defined above, is appropriate for the study of a static network signal.[1] If during the time evolution the graph structure stays the same, the time series associated to each vertex may simply be projected on the (generalized) eigenvectors as in the scalar case. However if the graph itself changes in time a more general framework must be used.

Consider a graph signal that evolves in (discrete) time. The corresponding graph would be, for each time t, a regular graph and each one of these graphs is forward-connected to the graph of the subsequent time. A vertex $v_n(t)$ at time t connects to the vertex $v_n(t+1)$ at time $t+1$. This construction accommodates the possible disappearance of vertices. In that case such vertex $v_n(t)$ would not have any forward edges. The connection of the vertices at time t to those at time $t+1$ and the signals $f_n(t)$ and $f_n(t+1)$ code for the dynamics of the signal, whereas the relation between the adjacency matrices $\mathbf{A}(t)$ and $\mathbf{A}(t+1)$ codes for the dynamics of the graph itself.

The construction of the $\mathbf{M}$-transforms and the graph tomograms will then proceed as before for the global adjacency matrix. To have a feeling for the kind of eigenvectors obtained for such adjacency matrices, consider a simple case of a finite-vertex circle graph with N vertices symmetrically connected to nearest-neighbors and forward connected in periodic time with τ time steps. Then, at each time t, the adjacency matrix $\mathbf{A}(t)$ is

$$\mathbf{A}(t) = \begin{pmatrix} 0 & 1 & 0 & 0 & \vdots & 1 \\ 1 & 0 & 1 & 0 & \vdots & 0 \\ 0 & 1 & 0 & 1 & \vdots & 0 \\ 0 & 0 & 1 & 0 & \vdots & 0 \\ \cdots & \cdots & \cdots & \cdots & \ddots & \vdots \\ 0 & 0 & 0 & \cdots & 1 & 0 \end{pmatrix}. \tag{31}$$

Let, for definiteness and notational simplicity, $N = \tau = 3$. Then the global 9×9 adjacency matrix is

$$\mathbf{A} = \begin{pmatrix} 0 & 1 & 1 & 0 & 0 & 0 & 1 & 0 & 0 \\ 1 & 0 & 1 & 0 & 0 & 0 & 0 & 1 & 0 \\ 0 & 1 & 0 & 0 & 0 & 0 & 0 & 0 & 1 \\ 1 & 0 & 0 & 0 & 1 & 1 & 0 & 0 & 0 \\ 0 & 1 & 0 & 1 & 0 & 1 & 0 & 0 & 0 \\ 0 & 0 & 1 & 0 & 1 & 0 & 0 & 0 & 0 \\ 0 & 0 & 0 & 1 & 0 & 0 & 0 & 1 & 1 \\ 0 & 0 & 0 & 0 & 1 & 0 & 1 & 0 & 1 \\ 0 & 0 & 0 & 0 & 0 & 1 & 0 & 1 & 0 \end{pmatrix}. \tag{32}$$

[1] Likewise, the usual time–frequency tomogram may be looked upon as a static description of the whole time history of the system.

This matrix is

$$\mathbf{A} = \left(\mathbf{I}_3 \otimes \begin{pmatrix} 0 & 1 & 1 \\ 1 & 0 & 1 \\ 0 & 1 & 0 \end{pmatrix}\right) \oplus \left(\left(\begin{pmatrix} 0 & 0 & 1 \\ 1 & 0 & 0 \\ 0 & 1 & 0 \end{pmatrix} \otimes \mathbf{I}_3\right)\right)$$

with eigenvalues

$$0,\ \frac{3 \pm \sqrt{5}}{2},\ \frac{-3 \pm \mathrm{i}\sqrt{3}}{2},\ \frac{-5 \pm \mathrm{i}\sqrt{3}}{2},\ \frac{5 \pm \mathrm{i}\sqrt{3}}{2}.$$

The "Fourier" transform of the dynamical graph signal will be the projection on the corresponding 9-dimensional eigenvectors.

For the construction of the tomogram, the vertex operator $\mathbf{T}$, as in (29), is

$$\mathbf{T} = \begin{pmatrix} \mathbf{T}^{(3)} & \mathbf{0} & \mathbf{0} \\ \mathbf{0} & \mathbf{T}^{(3)} & \mathbf{0} \\ \mathbf{0} & \mathbf{0} & \mathbf{T}^{(3)} \end{pmatrix}$$

where $\mathbf{T}^{(3)}$ is the 3×3 matrix $\begin{pmatrix} 1 & 0 & 0 \\ 0 & \mathrm{e}^{\mathrm{i}\frac{2\pi}{3}} & 0 \\ 0 & 0 & \mathrm{e}^{\mathrm{i}\frac{2\pi}{3}\times 2} \end{pmatrix}$.

This general framework, where one takes into account both the network edges and the time links, allows for a unified treatment of both the dynamics over graphs and the dynamics associated to a time changing topology.

4. Illustrative examples

In this section we present some examples of the use of graph transforms and graph tomograms. The detailed economic and biological implications of the examples are beyond the scope of this paper and will be reported elsewhere. The examples are included as an illustration of the concepts and also as a guide on how the graph formulation may be a powerful tool to analyze multivariate time series, in particular to detect weak correlations which might be undetectable by traditional clustering techniques.

4.1. A market network

An important problem in the design of portfolios or ETF's (Exchange Traded Funds) is the classification of the dynamical behavior of the trading values of market products. Identifying clusters of products with similar dynamical behavior allows the design of simpler portfolios, by the selection of representative elements in each cluster. Here we analyze the daily closing equity prices of 301 companies in the SP500 (Standard & Poors index) throughout the 250 trading days of 2012. For the purpose of the calculations the companies are ordered by sectors. For the benefit of the reader interested on detailed information on the companies used in this example their ticker symbols and GICS (Global Industry Classification Standard) sector codes are listed in the Appendix.

From the daily returns

$$r(t) = \log S(t) - \log S(t-1) \tag{33}$$

$S(t)$ being the closing price at day t, one computes a dynamical distance between the company stocks i and j by

$$d_{ij} = \sqrt{\sum_{t=1}^{250} \left(r_i(t) - r_j(t)\right)^2} \tag{34}$$

r_i and r_j being the return of companies i and j and the sum is over the 250 trading days in 2012.

Now one computes the smallest non-zero d_{ij} ($d_{\min}$) and an adjacency matrix $\mathbf{A}$ with matrix elements $\mathbf{A}_{ij}$ may be defined either by

$$\mathbf{A}^{\#}_{ij} = \frac{d_{\min}}{d_{ij}}\left(1 - \delta_{ij}\right) \tag{35}$$

or

$$\mathbf{A}^{(\beta)}_{ij} = \left(1 - \delta_{ij}\right) \exp\left(-\beta\left(d_{ij} - d_{\min}\right)\right). \tag{36}$$

The second form is sometimes the most convenient one because, by varying β, one obtains a multiscale analysis of the dynamical similarities of the companies. In Figs. 1 and 2 we show the color-coded adjacency matrices $\mathbf{A}^{\#}$ and $\mathbf{A}^{(\beta=2)}$ that are obtained. One sees that the $\mathbf{A}^{(\beta=2)}$-adjacency matrix provides a more detailed picture of the nature of correlations between

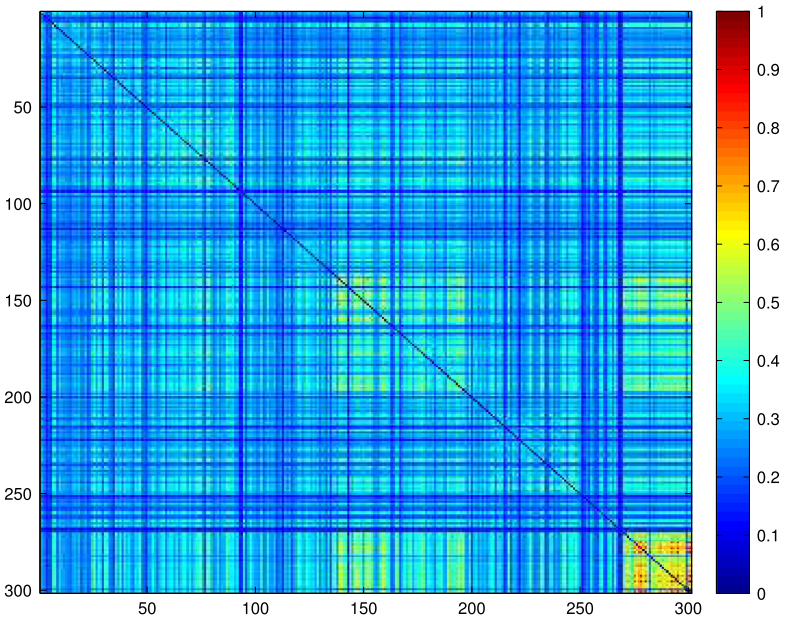

Fig. 1. Color-coded adjacency matrix $A^{\#}$ for the 301 companies. (For interpretation of the references to color in this figure legend, the reader is referred to the web version of this article.)

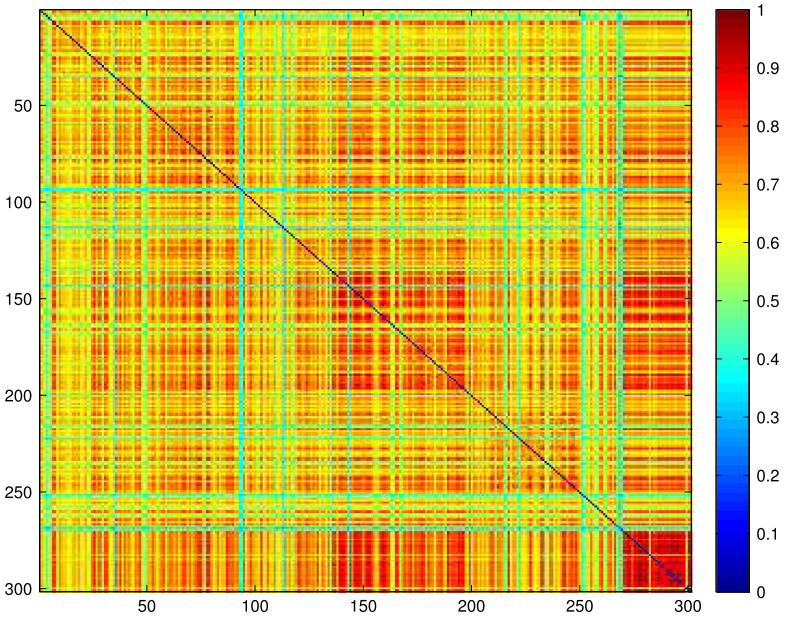

Fig. 2. Color-coded adjacency matrix $A^{(\beta)}$, $\beta = 2$, for the 301 companies. (For interpretation of the references to color in this figure legend, the reader is referred to the web version of this article.)

the return behavior of these equities. From inspection of this matrix one already sees that although the strongest correlations are on the "utilities" sector (GICS code 55), many other inter-sector correlations do exist. The main purpose of the analysis is precisely to identify sets of companies with similar return behavior.

For the remaining of our calculations we will use the $\mathbf{A}^{(\beta=2)} \triangleq \mathbf{A}$ as the adjacency matrix.

Now consider, as the signal on the graph, the yearly compound return

$$R_i = \prod_{t=1}^{250} (1 + r_i(t)) . \tag{37}$$

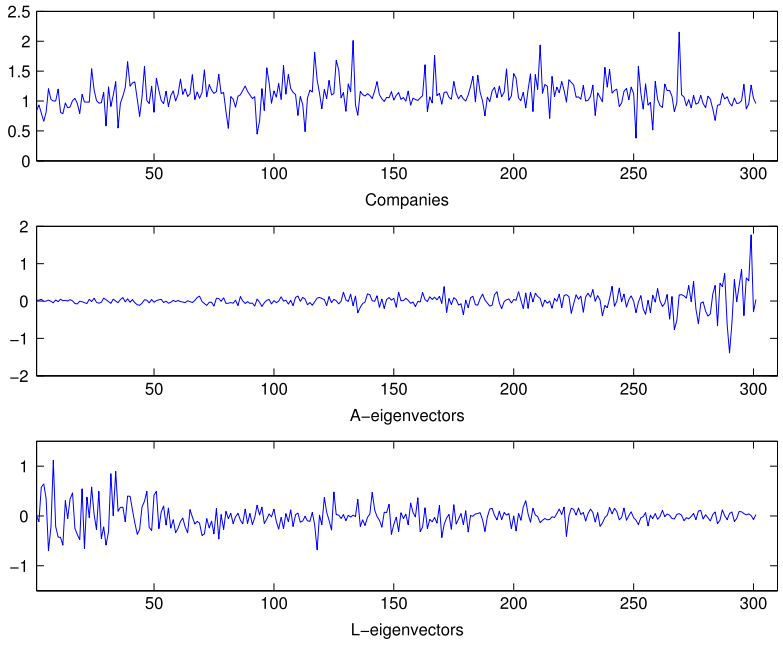

Fig. 3. The compound returns R_i and the absolute values of the projection of $R_i - \langle R_i \rangle$ on the eigenvectors of the adjacency and Laplacian matrices.

In Fig. 3 we compare the compound return R_i of the companies with the absolute value of the projections of $R_i - \langle R_i \rangle$ on the eigenvectors of the adjacency $\mathbf{A}$ and of the Laplacian $\mathbf{L} = \mathbf{D} - \mathbf{A}$ matrices. $\langle R_i \rangle$ is the mean value of the compound returns, which in this case was 1.1003.

One sees that the projection on the $\mathbf{A}$-eigenvectors (the $\mathbf{A}$-transform) is the one that provides a better information compression by selecting a smaller number of dominant eigenvectors.

For the purpose of comparison of the tomogram analysis, to be performed below, with a standard clustering technique, we consider the RatioCut technique [33]. This is a spectral technique which looks at the lowest non-zero eigenvalues in the spectrum of the Laplacian matrix, the corresponding eigenvectors leading (by K-means) to a division into clusters that minimizes the RatioCut

$$\text{RatioCut}\,(C_1, \ldots, C_K) = \frac{1}{2}\sum_{k=1}^{K} \frac{W\left(C_k, \overline{C_k}\right)}{|C_k|}$$

where $W\left(C_k, \overline{C_k}\right) = \sum_{i \in C_k, j \in \overline{C_k}} \mathbf{A}_{ij}$, $\overline{C_k}$ is the complement of the cluster C_k and $|C_k|$ is the number of elements in C_k.

From Fig. 4, where we have plotted the eigenvalues of the Laplacian matrix, one sees that in this case this criterion does not provide clear information on the cluster properties of the market network.

How the companies organize themselves into groups with similar return behavior is better understood by the examination of the $\mathbf{T}$, $\mathbf{A}$-tomogram (Fig. 5). Notice that here the vertex matrix $\mathbf{T}$ in addition to labeling the nodes also contains some more information, the companies being ordered by sectors. Fig. 5 is a contour plot of the absolute value of the projections of the compound return (Eq. (37)) on the eigenvectors of $B_\alpha = (1-\alpha)\,\mathbf{T} + \alpha \mathbf{A}^{(2)}$.

One sees how, starting from the compound return signal at $\alpha = 0$, the contributions of the companies organize themselves into clusters on the way to the final projection on the $\mathbf{A}$-eigenvectors (at $\alpha = 1$). The selection of clusters may be done by cutting the tomogram at diverse levels and reconstructing the components of the signal. All the signal information is contained at each α level. Therefore the signal components (dynamical clusters) are reconstructed by linear combinations of the eigenvectors around each peak with the coefficients taken from the tomogram. As an example Fig. 6 shows the cut at $\alpha = 0.85$ and Fig. 7 the reconstruction of the signal components around three of its peaks. The axis labeling corresponding to the ordered companies, clusters are simply identified by the strongest contributions.

One sees how these distinct dynamical clusters have important contributions from very different sectors. For example the last peak (components 298–300) is dominated by companies both in the utilities and the energy sector.

Comparing with the results of the RatioCut technique (Fig. 4) it seems that the tomographic analysis performs better at identifying clusters than the spectral technique. However, cluster identification here is simply based on the separation of the intensity peaks in the tomogram and we still lack an independent metric to analyze the fidelity of the detected clusters.

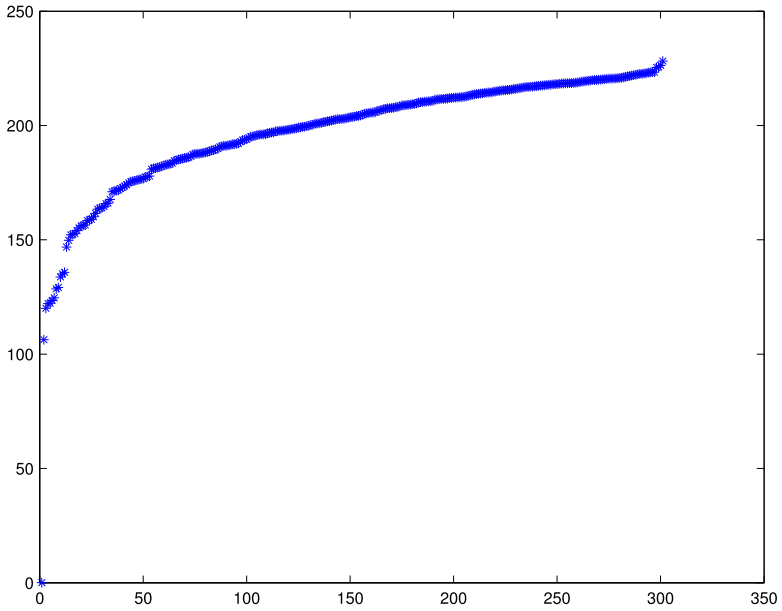

Fig. 4. Eigenvalues of the Laplacian matrix.

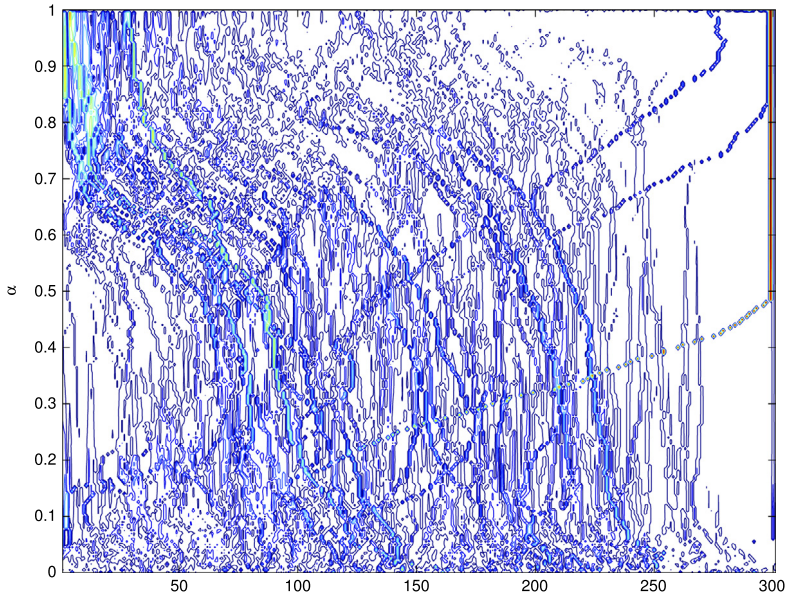

Fig. 5. The **T**, **A**-tomogram.

4.2. A trophic network

In this example, to be studied in more detail elsewhere, we analyze a biological network for which two types of information are available. It concerns 12 fish species of the North Sea for which we have information both on their trophic relations [40] and on their biomass evolution in the period 1976–2013, available at International Council for the Exploration of the Seas [41]. These species were selected for the availability of a relatively long biomass time series. The trophic relations, obtained from averaged stomach sampling are displayed in Fig. 8 and in the color-coded adjacency matrix $\mathbf{A}_{\text{troph}}$ of Fig. 9.

The ordered 12 species are: 1 = Cod adult; 2 = Whiting adult; 3 = Haddock adult; 4 = Saithe adult; 5 = Norway pout; 6 = Herring adult; 7 = Sprat; 8 = Sandeels; 9 = Plaice; 10 = Flounder; 11 = Sole; 12 = Lemon Sole.

Notice that in the $\mathbf{A}_{\text{troph}}$ matrix the lines do not sum up to one, because other species enter in the stomach data beyond the 12 considered here.

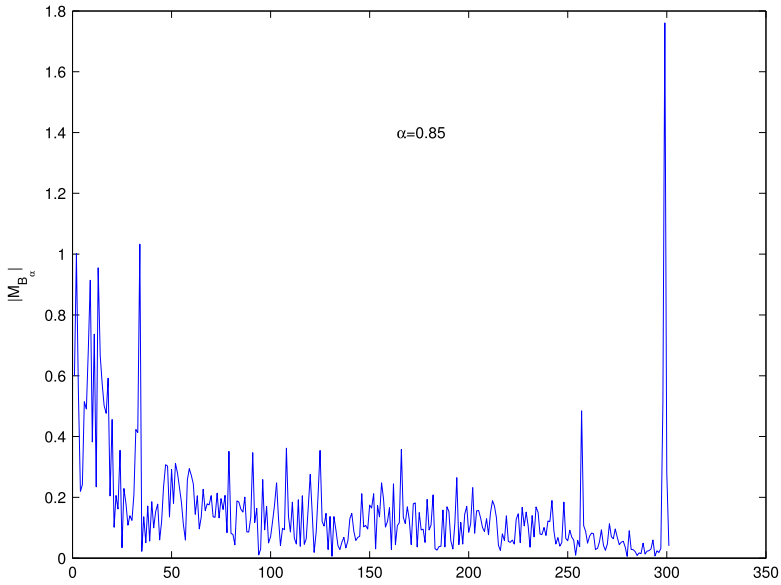

Fig. 6. The **T**, **A**-tomogram cut at $\alpha = 0.85$.

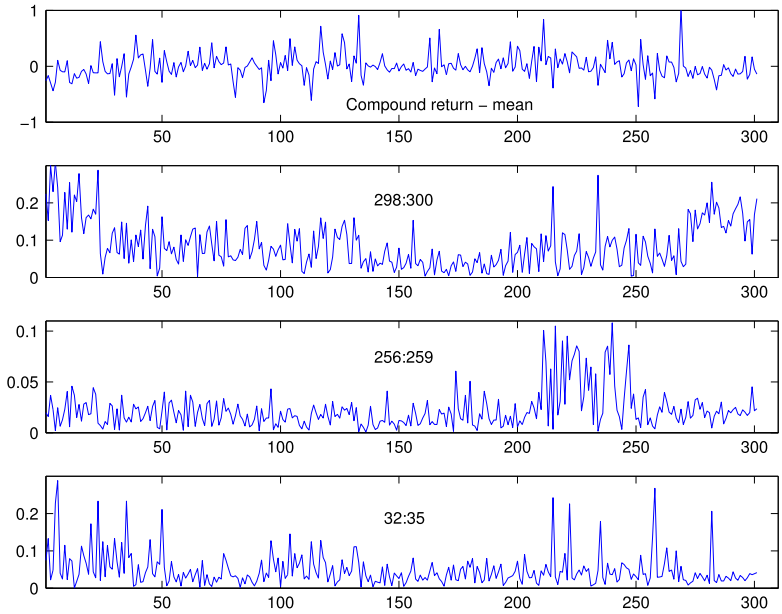

Fig. 7. The compound return and the absolute value of $R_i - \langle R_i \rangle$ for three different clusters in the tomogram.

For the analysis of the biomass time series $b\,(t)$, we consider the population growth rate as the most relevant variable [42]

$$r\,(t) = \log\left(\frac{b\,(t)}{b\,(t-1)}\right) \tag{38}$$

and define the Δ-delay distance function as

$$d_{ij}^{(\Delta)} = \sqrt{\sum_{t=\Delta}^{38} \left(r_i\,(t) - r_j\,(t-\Delta)\right)^2}. \tag{39}$$

The reason we consider time-delays for the growth rate distances is because in a trophic network the biomass is related to the other species offspring of previous years.

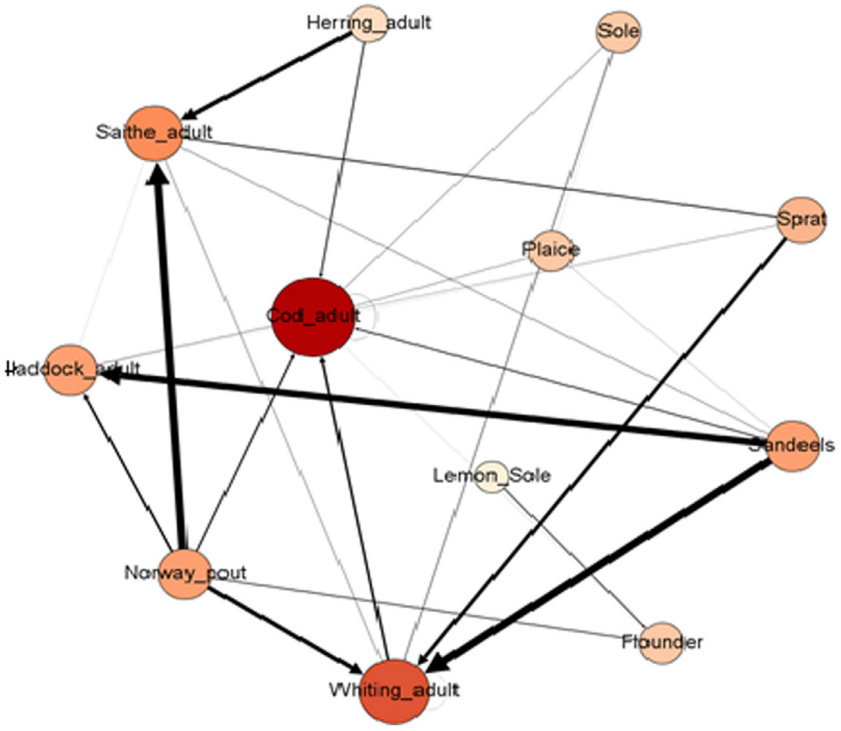

Fig. 8. North Sea Foodweb 12 species, directed and weighted.

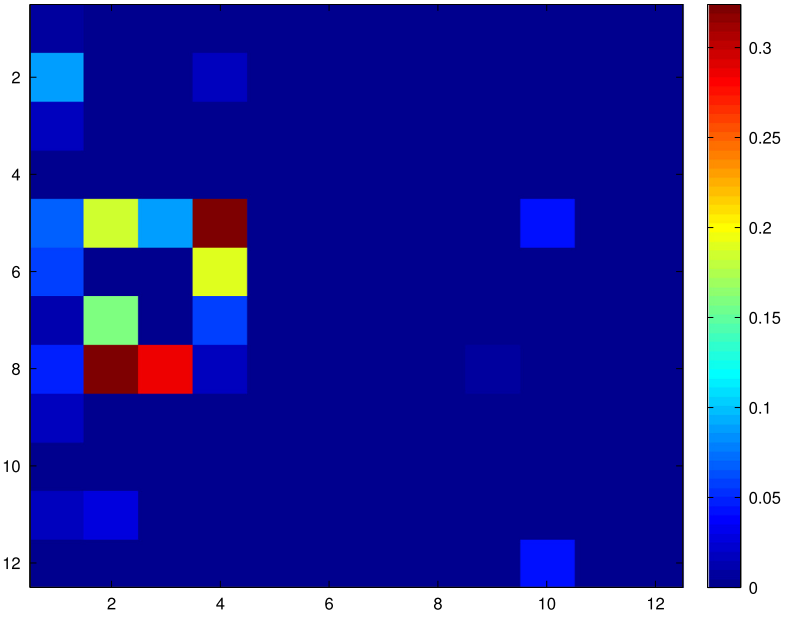

Fig. 9. Color-code trophic adjacency matrix $\mathbf{A}_{\text{troph}}$ for the 12 fish species. (For interpretation of the references to color in this figure legend, the reader is referred to the web version of this article.)

For each distance matrix, with elements $d_{ij}^{(\Delta)}$, we find the smallest nonzero element ($d_{\min}^{(\Delta)}$) and define biomass delayed adjacency matrices as

$$\mathbf{A}_{ij}^{(\Delta)} = \frac{d_{\min}^{(\Delta)}}{d_{ij}^{(\Delta)}}. \tag{40}$$

Fig. 10 displays the color-code one-year delayed biomass adjacency matrix.

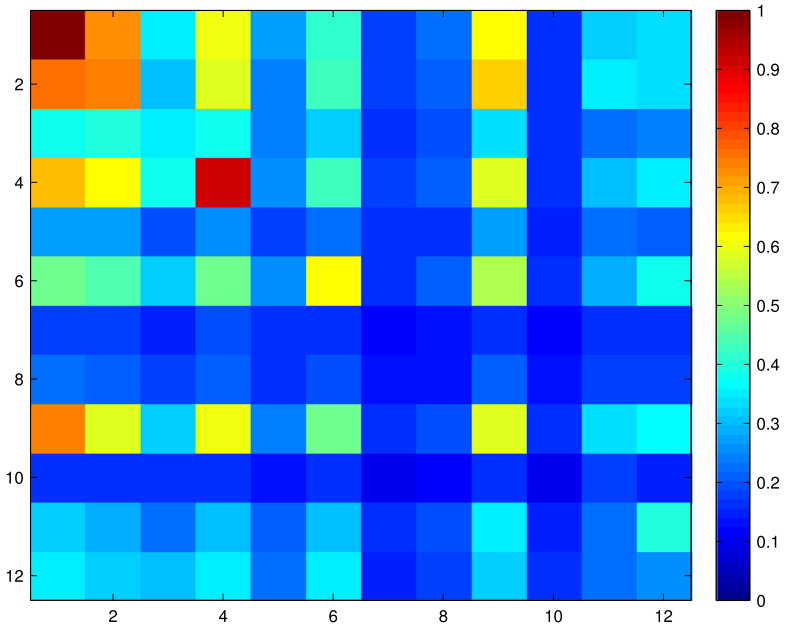

Fig. 10. Color-code one-year delayed biomass adjacency matrix. (For interpretation of the references to color in this figure legend, the reader is referred to the web version of this article.)

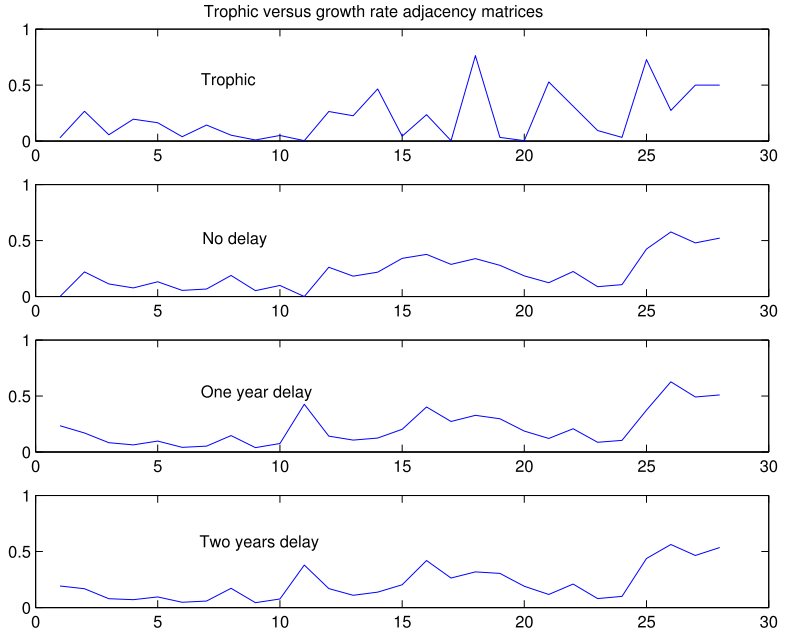

Fig. 11. Trophic versus growth rate adjacency matrices.

A simple inspection of Figs. 9 and 10 shows that the trophic and the biomass data do not contain the same information, which is to be expected since the biomass growth rate depends in many other factors besides predation. This is better seen in Fig. 11 where we have normalized to one each column in the trophic matrix, and then compared the 28 nonzero elements with the corresponding elements in the $\mathbf{A}_{ij}^{(\Delta)}$ matrices (also normalized to one).

Although some partial trends might be similar, the general conclusion is that the biomass growth rate evolution seems to depend on many other factors, different from the trophic relations of these 12 species.

In the remaining of this subsection we will use the one-year delayed biomass growth rate and the tomographic analysis to exhibit some of the interspecies correlations. Fig. 12 shows a contour plot of the tomogram corresponding to the operator $B = (1-\alpha)\,\mathbf{T}+\alpha\mathbf{A}^{(1)}\mathbf{A}^{(1)T}$. The signal that is projected on the eigenvectors of this operator is $R_i - \langle R_i\rangle$, R_i being the compound

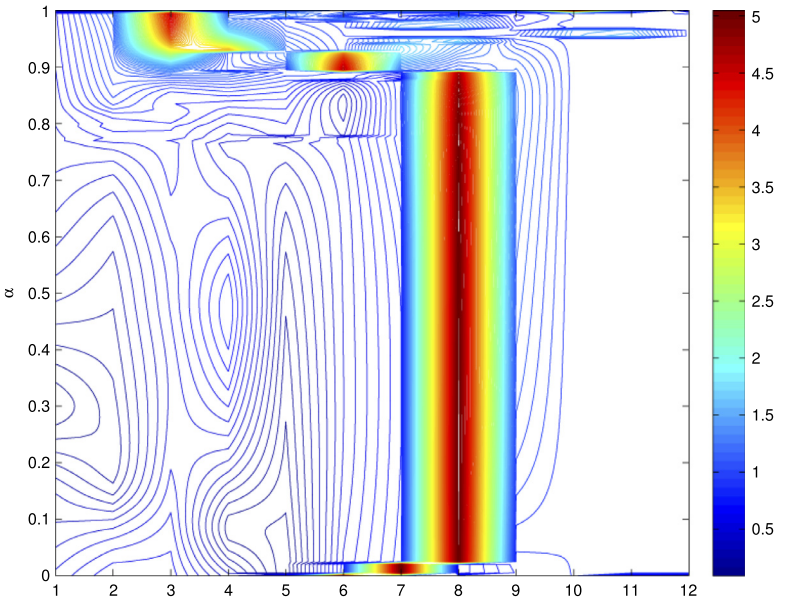

Fig. 12. The tomogram corresponding to the operator $B = (1-\alpha)\,\mathbf{T} + \alpha \mathbf{A}^{(1)}\mathbf{A}^{(1)T}$.

growth rate over 36 years

$$R_i = \prod_{t=1}^{36} (1 + r_i\,(t))\,.$$

The breaks that are observed in the contour plot result from the automatic ordering of the eigenvectors by ascending eigenvalue values. They are of no practical consequence, full information on the signal being kept at all α-levels. One sees how, for $\alpha \neq 0$ the signal information is compressed in a small number of eigenvectors.

As in the market network example, cutting the tomogram at intermediate α levels, clustering dependency of the species will be obtained. However, before doing it and for the purpose of comparison, we have attempted to apply the RatioCut technique. Because the one-year delayed matrices are not symmetric, we have plotted (Fig. 13) the eigenvalues of $\mathbf{L}\mathbf{L}^T$. One sees that except for the last eigenvalue they are all very small, suggesting non-existent or very weak correlations. Essentially, each time series would be a cluster by itself.

Nevertheless, the tomographic technique seems to be able to unravel some correlations, although admittedly weak. The upper plot in Fig. 14 shows a cut of the tomogram at $\alpha = 0.5$. One has a dominant peak at $X = 8$ and a smaller one at $X = 4$. Notice that these coordinates X do not correspond to the labeling of the species. It would be so only at $\alpha = 0$. To see what these correlations mean, one looks at the components of the eigenvectors of $B = (1-\alpha)\,\mathbf{T} + \alpha \mathbf{A}^{(1)}\mathbf{A}^{(1)T}$ at $\alpha = 0.5$ corresponding to these X values (the two lower plots in Fig. 14). The conclusion is that the dominant peak implies a (weak) correlation of species 4 (Saithe adult) with species 9 (Plaice) and the peak at $X = 4$ a correlation between species 3 (Haddock adult) and species 4 (Saithe adult).

5. Conclusions

1 —The growing set of big data associated to network phenomena motivates the development of new signal processing tools suited to the analysis of static and dynamical signals on graphs.
2 —Among the new tools, transforms like the generalization of Fourier transform have been developed. Other transforms may also be useful and, in this paper, a correct generalization of the wavelet transform has been constructed.
3 —For a multiple feature characterization of the signals a new graph tomographic transform is developed which, as in case of time series signals, is probabilistically robust.
4 —Two application examples are worked out where, in particular, tomograms are used for cluster identification. As far as internal correlations are concerned the two examples are of a very different nature. In the market data of SP500 there are strong correlations. This is well known and is at the basis of the construction of portfolios. The most interesting fact is that, as highlighted in the paper, these correlations most times involve companies in quite different sectors.

In the second example, for the fish populations, the correlations are weak, but whereas other classical methods (RatioCut, etc.) are unable to detect them, the tomographic technique may nevertheless identify some relevant ones.

In any case the examples are merely illustrative and the core of the paper is the set of robust analyzing techniques that are developed, which may be useful for network phenomena in many fields.

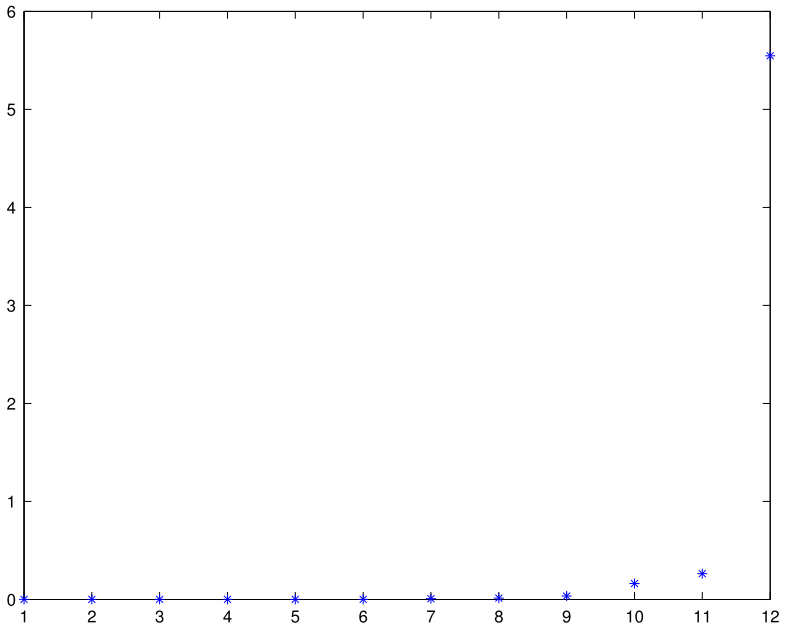

Fig. 13. Eigenvalues of $\mathbf{L}\mathbf{L}^T$.

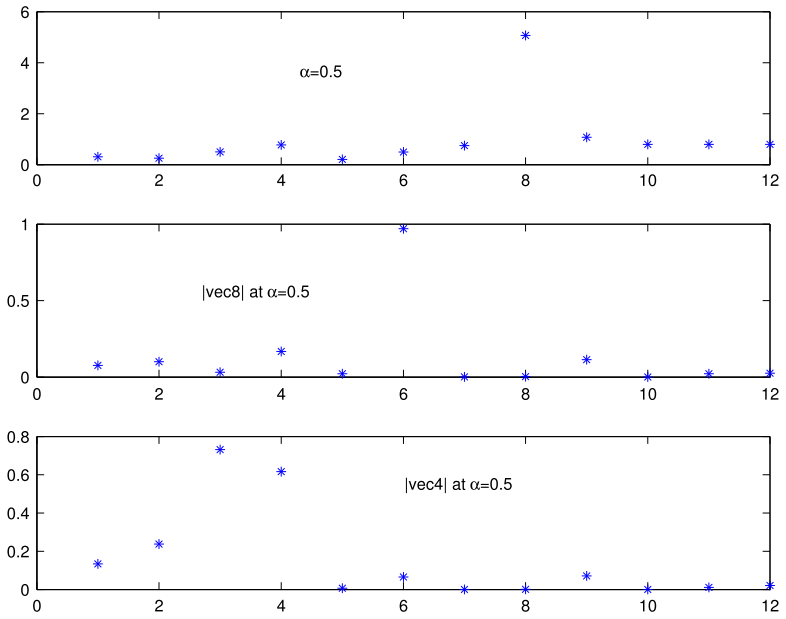

Fig. 14. Cut of the tomogram at $\alpha = 0.5$ (upper plot) and the eigenvector components corresponding to the peaks at $X = 8$ and $X = 4$.

Appendix. Ticker symbols and GICS sector codes of the SP500 companies used in the example of 4.1

APA(10); APC(10); BHI(10); CHK(10); CNX(10); COG(10); COP(10); CVX(10); DNR(10); DO(10); DVN(10); FTI(10); HAL(10); HES(10); HP(10); MRO(10); NBL(10); NOV(10); OXY(10); PXD(10); RDC(10); SLB(10); SWN(10); VLO(10); WMB(10); XOM(10); AA(15); APD(15); ARG(15); ATI(15); BLL(15); BMY(15); CAM(15); CF(15); CLF(15); DD(15); DOW(15); ECL(15); EMN(15); IFF(15); IP(15); MON(15); MUR(15); NEM(15); NUE(15); PPG(15); PX(15); SEE(15); VMC(15); X(15); APH(20); AVY(20); BA(20); CAT(20); CMI(20); CSX(20); DE(20); DHR(20); DNB(20); DOV(20); EFX(20); EMR(20); ETN(20); FDX(20); FLR(20); FLS(20); GD(20); GE(20); GWW(20); HON(20); IR(20); IRM(20); ITW(20); LLL(20); LMT(20); LUV(20); MAS(20); MMM(20); NOC(20); NSC(20); PBI(20); PH(20); PLL(20); R(20); RHI(20); ROK(20); RTN(20); TYC(20); UNP(20); UTX(20); AN(25); AZO(25); BBY(25); BIG(25); CCE(25); COH(25); DFS(25); DIS(25); DRI(25); F(25); FDO(25); GCI(25); GPC(25); GPS(25); HAR(25); HD(25); HOG(25); HOT(25); HRB(25); IGT(25); IPG(25); JCI(25); JCP(25); JWN(25); KMX(25);

LEG(25); LEN(25); LOW(25); LTD(25); MCD(25); MHP(25); NKE(25); NWL(25); OMC(25); PCP(25); SHW(25); SNA(25); SWK(25); TGT(25); TIF(25); TJX(25); VFC(25); WHR(25); ADM(30); AVP(30); BFb(30); CAG(30); CCL(30); CL(30); CLX(30); CPB(30); CVS(30); DF(30); DPS(30); EL(30); GIS(30); HNZ(30); HRL(30); HSY(30); JEC(30); K(30); KMB(30); KO(30); KR(30); LO(30); M(30); MJN(30); MO(30); PEP(30); PG(30); PM(30); SJM(30); STZ(30); SWY(30); SYY(30); TAP(30); TSO(30); WAG(30); WMT(30); WPO(30); ABC(35); ABT(35); AET(35); AGN(35); BAX(35); BCR(35); BDX(35); BMS(35); BSX(35); CAH(35); CFN(35); CI(35); CVH(35); DGX(35); DVA(35); FRX(35); HSP(35); HUM(35); JNJ(35); LH(35); LLY(35); MCK(35); MDT(35); MKC(35); MRK(35); PFE(35); PKI(35); STJ(35); SYK(35); THC(35); TMO(35); UNH(35); VAR(35); WAT(35); WLP(35); AFL(40); AIG(40); AIZ(40); ALL(40); AXP(40); BAC(40); BBT(40); BEN(40); BK(40); BTU(40); C(40); CB(40); CBG(40); CMA(40); COF(40); FHN(40); GNW(40); GS(40); HIG(40); JPM(40); KEY(40); L(40); LM(40); LNC(40); LUK(40); MET(40); MMC(40); MTB(40); NBR(40); NYX(40); PGR(40); PNC(40); RF(40); SCHW(40); STI(40); STT(40); TMK(40); TRV(40); TSN(40); UNM(40); USB(40); WFC(40); WM(40); XL(40); A(45); AMD(45); CSC(45); EMC(45); FCX(45); FIS(45); GLW(45); GME(45); HPQ(45); HRS(45); IBM(45); JBL(45); JNPR(45); MA(45); MWV(45); TER(45); TSS(45); XRX(45); PCS(50); S(50); T(50); VZ(50); AEE(55); AEP(55); AES(55); CMS(55); CNP(55); D(55); DTE(55); DUK(55); ED(55); EIX(55); EQT(55); ETR(55); EXC(55); FE(55); GAS(55); NEE(55); NI(55); NU(55); PCG(55); PEG(55); PNW(55); POM(55); PPL(55); SCG(55); SRE(55); TE(55); TEG(55); TXT(55); WEC(55); XEL(55).

References

[1] F.R.K. Chung, Spectral Graph Theory, American Mathematical Society, Providence, 1997.
[2] B.A. Miller, N.T. Bliss, P.J. Wolfe, Towards signal processing theory for graphs and non-Euclidean data, in: Proc. ICASSP, 2010, pp. 5414–5417.
[3] D.I. Shuman, et al., The emerging field of signal processing on graphs. Extending high-dimensional data analysis to networks and other irregular domains, IEEE Signal Process. Mag. 30 (2013) 83–98.
[4] A. Sandryhaila, J.F. Moura, Discrete signal processing on graphs, IEEE Trans. Signal Process. 61 (2013) 1644–1656.
[5] A. Sandryhaila, J.F. Moura, Discrete signal processing on graphs: Frequency analysis, IEEE Trans. Signal Process. 62 (2014) 3042–3054.
[6] A. Sandryhaila, J.F. Moura, Big data analysis with signal processing on graphs, IEEE Signal Process. Mag. 31 (2014) 80–90.
[7] V.N. Ekambaram, G.C. Fanti, B. Ayazifar, K. Ramchandran, Circulant structures and graph signal processing, in: 20th IEEE Int. Conf. on Image Processing, ICIP, 2013, pp. 834–838.
[8] V.I. Man'ko, R. Vilela Mendes, Noncommutative time–frequency tomography, Phys. Lett. A 263 (1999) 53–59.
[9] M.A. Man'ko, V.I. Man'ko, R. Vilela Mendes, Tomograms and other transforms: A unified view, J. Phys. A: Math. Gen. 34 (2001) 8321–8332.
[10] F. Briolle, V.I. Man'ko, B. Ricaud, R. Vilela Mendes, Non-commutative tomography: A tool for data analysis and signal processing, J. Russ. Laser Res. 33 (2012) 103–121.
[11] C. Aguirre, R. Vilela Mendes, Signal recognition and adapted filtering by non-commutative tomography, IET Signal Process. 8 (2014) 67–75.
[12] A.D. Poularikas (Ed.), The Transforms and Applications Handbook, CRC Press & IEEE Press, Boca Raton, Florida, 1996.
[13] K.-B. Wolf, Integral Transforms in Science and Engineering, Plenum Press, New York, 1979.
[14] E. Wigner, On the quantum correction for thermodynamic equilibrium, Phys. Rev. 40 (1932) 749–759.
[15] J. Ville, Théorie et applications de la notion de signal analytique, Cables Transm. 2A (1948) 61–74.
[16] J. Bertrand, P. Bertrand, A class of affine Wigner functions with extended covariance properties, J. Math. Phys. 33 (1992) 2515–2527.
[17] P. Goncalvés, R.G. Baraniuk, A pseudo-Bertrand distribution for time–scale analysis, IEEE Signal Process. Lett. 3 (1996) 82–84.
[18] L. Cohen, Generalized phase-space distribution functions, J. Math. Phys. 7 (1996) 781–806.
[19] L. Cohen, Time–frequency distributions. A review, Proc. IEEE 77 (1989) 941–981.
[20] S. Qian, D. Chen, Joint Time–Frequency Analysis, Prentice-Hall, Englewood Cliffs, NJ, 1995.
[21] K. Husimi, Some formal properties of the density matrix, Proc. Phys. Mat. Soc. Jpn 22 (1940) 264–314.
[22] Y. Kano, A new phase-space distribution function in the statistical theory of the electromagnetic field, J. Math. Phys. 6 (1965) 1913–1915.
[23] S.R. Deans, The Radon Transform and Some of its Applications, John Wiley & Sons, New York, 1983.
[24] J.C. Woods, D.T. Barry, Linear signal synthesis using the Radon–Wigner transform, IEEE Trans. Signal Process. 42 (1994) 2105–2111.
[25] S. Granieri, W.D. Furlan, G. Saavedra, P. Andrés, Radon–Wigner display: a compact optical implementation with a single varifocal lens, Appl. Opt. 36 (1997) 8363–8369.
[26] A. Böhm, M. Gadella, Dirac Kets, Gamow Vectors and Gel'fand Triplets, Springer-Verlag, New York, 1989.
[27] F. Briolle, R. Lima, V.I. Man'ko, R. Vilela Mendes, A tomographic analysis of reflectometry data I: Component factorization, Meas. Sci. Technol. 20 (2009) 105501.
[28] F. Briolle, R. Lima, R. Vilela Mendes, A tomographic analysis of reflectometry data II: The phase derivative, Meas. Sci. Technol. 20 (2009) 105502.
[29] F. Clairet, F. Briolle, B. Ricaud, S. Heuraux, New signal processing technique for density profile reflectometry on Tore Supra, Rev. Sci. Instrum. 82 (2011) 083502.
[30] B. Ricaud, F. Briolle, F. Clairet, Analysis and separation of time–frequency components in signals with chaotic behavior, arXiv:1003.0734.
[31] C. Aguirre, P. Pascual, D. Campos, E. Serrano, Single neuron transient activity detection by means of tomography, BMC Neurosci. 12 (Suppl. 1) (2011) 297–298.
[32] A. Agaskar, Y.M. Lu, Uncertainty principles for signals defined on graphs: Bounds and characterizations, in: 2012 IEEE Int. Conf. on Acoustics, Speech and Signal Processing, ICASSP, 2012, pp. 3493–3496.
[33] U. Von Luxburg, A tutorial on spectral clustering, Stat. Comput. 17 (2007) 395–416.
[34] F. Krzakala, C. Moore, E. Mossel, J. Neeman, A. Sly, L. Zdeborova, Spectral redemption in clustering sparse networks, http://dx.doi.org/10.1073/pnas.1312486110.
[35] R. Nadakuditi, M. Newman, Graph spectra and the detectability of community structure in networks, Phys. Rev. Lett. 108 (2012) 188701.
[36] K. Hashimoto, Zeta functions of finite graphs and representation of p-adic groups, Adv. Stud. Pure Math. 15 (1989) 211–280.
[37] M. Newman, Finding community structure in networks using the eigenvectors of matrices, Phys. Rev. E74 (2006) 036104.
[38] D.K. Hammond, P. Vandergheynst, R. Gribonval, Wavelets on graphs via spectral graph theory, Appl. Comput. Harmon. Anal. 30 (2011) 129–150.
[39] A. Agaskar, YueM. Lu, A spectral graph uncertainty principle, IEEE Trans. Inform. Theory 59 (2013) 4338–4356.
[40] S. Mackinson, G. Daskalov, An ecosystem model of the North Sea to support an ecosystem approach to fisheries management: description and parameterization, in: Sci. Ser. Tech. Rep., Cefas Lowestoft, 142, 2007, 196 pp.
[41] http://www.ices.dk/community/advisory-process/Pages/Latest-Advice.aspx.
[42] H.-S. Niwa, Random-walk dynamics of exploited fish populations, ICES J. Mar. Sci. 64 (2007) 496–502.